Angular Analysis of $B_d^0 \to K^{*0}\mu^+\mu^-$ with the ATLAS Experiment

Anna Usanova*

on behalf of the ATLAS Collaboration

Innsbruck University

E-mail: anna.usanova@uibk.ac.at

A measurement of the muon forward-backward asymmetry A_{FB} and the fraction of the K^{*0} longitudinal polarisation F_L in the decay $B_d^0 \to K^{*0}\mu^+\mu^-$ is presented. The data used was collected with the ATLAS detector at the Large Hadron Collider in proton-proton collisions at a centre of mass energy of $\sqrt{s} = 7\,\text{TeV}$ in the year 2011 and amounts to $4.9\,\text{fb}^{-1}$ of integrated luminosity. The measurement is compared to the predictions of the Standard Model and the results of other experiments.

14th International Conference on B-Physics at Hadron Machines
April 8-12, 2013
Bologna, Italy

---

*Speaker.

1. Introduction

The $B_d^0 \to K^{*0}\mu^+\mu^-$ decay is one of the exclusive final states of the $b \to s\ell^+\ell^-$ transition that in lowest order occurs only via loop level diagrams within the Standard Model and therefore has a small branching fraction of $(1.06 \pm 0.1) \cdot 10^{-6}$ [1]. The decay amplitudes and the angular distributions of the 4-particle final state are sensitive to the effects of physics beyond the Standard Model [2].

The $B_d^0 \to K^{*0}(\to K^+\pi^-)\mu^+\mu^-$ process can be described by four kinematic variables. One is the invariant mass q^2 of the di-muon system, the other three are the angles describing the kinematical configuration of the final state which are shown in Figure 1. These angles are θ_L - the angle between the μ^+ and the direction opposite to the B_d^0 in the di-muon rest frame, θ_K - the angle between the K^+ and the direction opposite to the B_d^0 in the K^{*0} rest frame, and ϕ - the angle between the di-muon plane and the plane defined by the kaon-pion system in the B_d^0 rest frame. For the $\overline{B}_d^0$ decay the angles θ_L and θ_K are defined with respect to the μ^- and the K^-. The differential decay
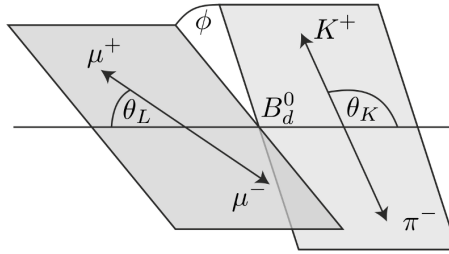
Figure 1: Definition of the kinematic angles in the decay $B_d^0 \to K^{*0}\mu^+\mu^-$. Figure taken from [3].

rate is a function of these four variables. In case of insufficient statistics two of the angles can be integrated out, resulting in the 2-dimensional distributions $\mathrm{d}^2\Gamma/\mathrm{d}q^2\mathrm{d}\cos\theta_L$ and $\mathrm{d}^2\Gamma/\mathrm{d}q^2\mathrm{d}\cos\theta_K$. This article describes the measurement of the forward-backward asymmetry of the muons A_{FB} and the fraction of the K^{*0} longitudinal polarisation F_L obtained from the fits to 1-dimensional angular distributions, while the dependence on the q^2 is accounted for by performing the fit in several ranges of di-muon mass and assuming that the A_{FB} and F_L values stay constant within each range [3]. The forward-backward asymmetry is defined as $A_{FB} = (N_F - N_B)/(N_F + N_B)$, where N_F is the number of muons going in the forward direction in the di-muon rest frame and N_B is the number of muons going in the backward direction, and the K^{*0} mesons with zero projection of the spin on the direction of motion are referred to as "longitudinally polarised".

2. Event selection

For this analysis $4.9\,\mathrm{fb}^{-1}$ of data from pp-collisions at $\sqrt{s} = 7$ TeV collected by the ATLAS detector at the LHC in 2011 were used. Samples of Monte Carlo events have been generated with PYTHIA for the signal decay channel $B_d^0 \to K^{*0}\mu^+\mu^-$, the resonant background decay channel $B_d^0 \to K^{*0}J/\psi$, Drell-Yan process and for $b\bar{b} \to \mu^+\mu^- X$ and $c\bar{c} \to \mu^+\mu^- X$ processes contributing to the continuum background.

Several triggers, either single-muon or di-muon ones, were used to select the events. The main triggers select di-muon events requiring both muons to have $p_T(\mu) > 4\,\mathrm{GeV}$, or alternatively

$p_T(\mu_1) > 6\,\text{GeV}$ and $p_T(\mu_2) > 4\,\text{GeV}$. Each of the events was required to be recorded by at least one of the selected triggers.

Two sets of cuts are applied on the data — baseline cuts (general requirements to ensure good measurement quality) and selection cuts, the values of which are optimised for the analysis. Baseline cuts include the requirement for all four tracks to have pseudorapidity $|\eta| < 2.5$, transverse momentum p_T of muons to be above 3.5 GeV and p_T of kaons and pions above 0.5 GeV. Two muon tracks refitted to a common vertex must satisfy $\chi^2/\text{ndf} < 10$. The mass of K^{*0} candidates must be between 846 MeV and 946 MeV.

The selection cuts are optimised by maximizing the estimator $\mathscr{P} = N_{sig}/\sqrt{N_{sig} + N_{bckg}}$, where N_{sig} is the number of selected signal events and N_{bckg} the number of background events. The optimization is performed using Monte Carlo events only. A cut on the lifetime significance of $\tau/\sigma_\tau > 12.75$ is imposed to remove most of $b\bar{b} \to \mu^+\mu^- X$, $c\bar{c} \to \mu^+\mu^- X$ and Drell-Yan events. A cut on the pointing angle $\cos\theta > 0.999$ is effective against the combinatorial background. Here θ is defined as the angle between the reconstructed 3-momentum vector of the B_d^0 candidate and its reconstructed direction of flight, i.e. the vector between the primary vertex and the reconstructed B_d^0 vertex. A quality requirement is applied to the reconstructed B_d^0 vertex, $\chi^2/\text{ndf} < 2$. Background events with K^{*0} candidates which do not originate from a B decay are removed by the cut on the K^{*0} transverse momentum, $p_T(K^{*0}) > 3.0\,\text{GeV}$. To remove the $B_d^0 \to K^{*0}J/\psi$ and $B_d^0 \to K^{*0}\psi(2S)$ events with the subsequent decay of the charmonium into a photon and two muons (e.g. $J/\psi \to \gamma\mu^+\mu^-$ or $\psi(2S) \to \gamma\mu^+\mu^-$), a cut $|(m(B_d^0)_{rec} - m(B_d^0)_{PDG}) - (m(\mu^+\mu^-)_{rec} - m(J/\psi)_{PDG})| = \Delta m < 130$ MeV is applied (similar to CDF [4]). This requirement was also found to be effective against the remaining J/ψ and $\psi(2S)$ in the tails of the charmonium peaks.

The mass distribution of the events satisfying all these requirements is shown in Figure 2.
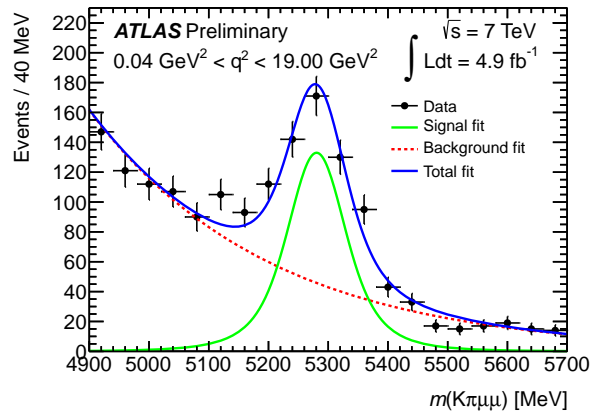
Figure 2: Invariant mass distribution of $B_d^0 \to K^{*0}\mu^+\mu^-$ candidates as data points after the full signal selection. The solid blue (dark) line denotes the mass likelihood fit, the dotted red line - its background component and the solid green (light) line - the signal component. Figure taken from [3].

3. Analysis strategy

Since the longitudinal polarisation fraction F_L and the lepton forward-backward asymmetry

A_{FB} are the functions of di-muon invariant mass q^2, the data is separated into several regions of q^2, and the averaged F_L and A_{FB} values are obtained independently in each of the q^2 bins.

The values for A_{FB} and F_L are extracted by performing a sequential unbinned maximum likelihood fit, where in a first step the invariant $K\pi\mu\mu$ mass distribution is fitted, then the resulting parameters are fixed, and in a second step - where the number of signal events is fixed by the previous fit - the angular distributions are fitted. The likelihood function for the invariant mass distribution is written as

$$\mathscr{L} = \prod_{i=1}^{N} \left[N_{\text{sig}} \cdot \mathscr{M}_{\text{sig}}(m_i, \delta_{m_i}) + N_{\text{bckg}} \cdot \mathscr{M}_{\text{bckg}}(m_i) \right], \tag{3.1}$$

where N_{sig} and N_{bckg} are the number of signal and background events, $\mathscr{M}_{\text{sig}}$ and $\mathscr{M}_{\text{bckg}}$ are the probability density functions for signal and background, respectively, and $N_{sig} + N_{bckg}$ is the Poisson distributed expected number of total events. The probability density function for signal is described by a Gaussian function with mass m_i and per-candidate error δ_{m_i} and for the background by an exponential function.

The differential decay rate of $B_d^0 \to K^{*0}\mu^+\mu^-$ is a function of the invariant di-muon mass q^2 and the three helicity angles θ_L, θ_K and ϕ in the rest frame of the four particle final state. At a given q^2 its integration over θ_K and ϕ gives [5, 6]

$$\frac{1}{\Gamma}\frac{\mathrm{d}^2\Gamma}{\mathrm{d}q^2\mathrm{d}\cos\theta_L} = \frac{3}{4}F_L(q^2)\left(1 - \cos^2\theta_L\right) +$$
$$\frac{3}{8}\left(1 - F_L(q^2)\right)\left(1 + \cos^2\theta_L\right) + A_{FB}(q^2)\cos\theta_L \tag{3.2}$$

and the integration over θ_L and ϕ of the differential decay rate yields

$$\frac{1}{\Gamma}\frac{\mathrm{d}^2\Gamma}{\mathrm{d}q^2\mathrm{d}\cos\theta_K} = \frac{3}{2}F_L(q^2)\cos^2\theta_K + \frac{3}{4}\left(1 - F_L(q^2)\right)\left(1 - \cos^2\theta_K\right). \tag{3.3}$$

Fixing the parameters obtained in the invariant mass fit, the likelihood function for the angular distributions is written as

$$\mathscr{L} = \prod_{i=1}^{N}[N_{\text{sig}}^{fix} \cdot \mathscr{M}_{\text{sig}}(m_i, \delta_{m_i}) \cdot \mathscr{A}_{L,\text{sig}}(\cos\theta_{L,i}) \cdot \alpha_L(\cos\theta_{L,i}) \cdot \mathscr{A}_{K,\text{sig}}(\cos\theta_{K,i}) \cdot \alpha_K(\cos\theta_{K,i}) +$$
$$N_{\text{bckg}}^{fix} \cdot \mathscr{M}_{\text{bckg}}(m_i) \cdot \mathscr{A}_{L,\text{bckg}}(\cos\theta_{L,i}) \cdot \mathscr{A}_{K,\text{bckg}}(\cos\theta_{K,i})], \tag{3.4}$$

where the $\mathscr{A}$'s denote the probability density functions of the angular distributions of $\cos\theta_K$ and $\cos\theta_L$ for the signal and the background. The angular distributions of the signal are given by Equations (3.2) and (3.3), and those for the background are modelled with the second order Chebyshev polynomials. To take into account angular detector efficiencies due to trigger, event reconstruction, detector effects and the selection cuts, the angular signal distributions are multiplied by acceptance functions α_K and α_L. To determine the acceptance functions a signal Monte Carlo sample with full detector simulation and uniform distribution of helicity angles was generated. The acceptance functions were obtained by the fit to $\cos\theta_K$ and $\cos\theta_L$ distributions in this sample after applying all the baseline and selection cuts.

4. Systematics

Various sources of systematic uncertainties are taken into account, evaluated for each q^2 bin separately. The possible impact of the sequential fitting procedure on the final results was estimated by comparing the sequential mass and angular unbinned maximum likelihood fit with the combined mass-angular fit. Deviations in the B_d^0 invariant mass fit due to the cut on $\Delta m < 130$ MeV are accounted for by varying the B_d^0 mass fit region. Several possible effects of the angular acceptance functions were studied. First, variations of the acceptance functions due to limited statistics of the used Monte Carlo sample were investigated. Second, the effect of the correlations among the full three angles using the angular distributions were studied with signal Monte Carlo samples produced with the angular distributions predicted by the Standard Model [7] and measured by LHCb [8]. Finally the effect of acceptance and resolution in the di-muon mass was estimated. Next, two muons and each of the hadronic tracks were combined to test the hypothesis that they originate from a $B^\pm \to K^\pm \mu^+\mu^-$ decay. All potential $B^\pm$ candidates were removed from the final data sample, impact on the fit result is assigned as systematic uncertainty.

Several possible contributions to the systematic uncertainty were studied and found negligible. One of them is the presense of S-wave (i.e. $B_d^0 \to K^+\pi^-\mu^+\mu^-$ decays), which has a negligible effect on the angular distributions, assuming an 8% S-wave contribution (estimated by BaBar [9]). No events with $K\pi\mu\mu$ invariant mass compatible with B_s^0 one were found, therefore the possible contribution of $B_s^0 \to \phi\mu^+\mu^-$ decay is also negligible.

There is no common dominating source of systematic uncertainty for all of the q^2-bins, the largest contribution varies among the bins. For the 2.00 GeV$^2 < q^2 < 4.30$ GeV^2 range, the sequential fit procedure has the largest effect due to low statistics in this bin. The results in the central bin are mostly affected by the choice of fit region, since the Δm cut removes a lot of events in the sidebands in this range of di-muon mass. In all of the q^2-bins the statistical uncertainty dominates over the systematical one.

q^2 range (GeV^2)	N_{sig}	A_{FB}	F_L
$2.00 < q^2 < 4.30$	19 ± 8	$0.22 \pm 0.28 \pm 0.14$	$0.26 \pm 0.18 \pm 0.06$
$4.30 < q^2 < 8.68$	88 ± 17	$0.24 \pm 0.13 \pm 0.01$	$0.37 \pm 0.11 \pm 0.02$
$10.09 < q^2 < 12.86$	138 ± 31	$0.09 \pm 0.09 \pm 0.03$	$0.50 \pm 0.09 \pm 0.04$
$14.18 < q^2 < 16.00$	32 ± 14	$0.48 \pm 0.19 \pm 0.05$	$0.28 \pm 0.16 \pm 0.03$
$16.00 < q^2 < 19.00$	149 ± 24	$0.16 \pm 0.10 \pm 0.03$	$0.35 \pm 0.08 \pm 0.02$
$1.00 < q^2 < 6.00$	42 ± 11	$0.07 \pm 0.20 \pm 0.07$	$0.18 \pm 0.15 \pm 0.03$

Table 1: Summary of the fit results for the different bins of q^2. Number of signal events N_{sig} from the mass fit and its statistical uncertainty, forward backward asymmetry A_{FB} and longitudinal polarisation F_L for different bins in q^2 including statistical and systematic uncertainties.

5. Results

The parameters A_{FB} and F_L are extracted in the six ranges of di-muon mass. The final re-

sults of the unbinned maximum likelihood fit including statistical and systematic uncertainties are summarised in Table 1. No results are present in 0.04 GeV^2 to 2.00 GeV^2 bin due to unsufficient statistics. In Figures 3 and 4 the measurements of ATLAS are compared to the measurements of other experiments and the Standard Model. The theoretical expectations have been calculated for the limit of small [5] and large [6] vector meson energy, no prediction is given for the central q^2 region. ATLAS results are in general agreement with those of the other experiments. A small deviation from the Standard Model prediction for F_L is observed in the first two bins of q^2, but the difference is not significant.
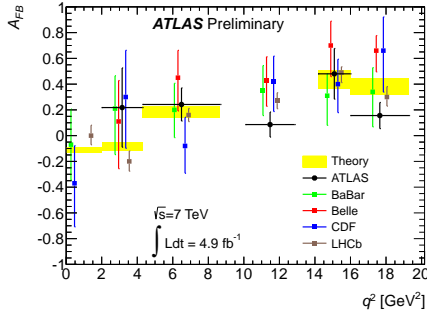
Figure 3: Forward-backward asymmetry of the muons A_{FB}, including statistical and systematic uncertainties, compared to theoretical predictions [7] and results of BaBar [10], Belle [11], CDF [12] and LHCb [8]. Figure taken from [3].
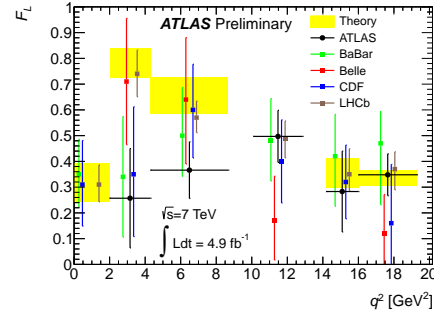
Figure 4: Fraction of longitudinally polarised K^{*0} mesons, F_L, including statistical and systematic uncertainties, compared to theoretical predictions [7] and results of BaBar [10], Belle [11], CDF [12] and LHCb [8]. Figure taken from [3].

6. Acknowledgements

References

[1] Particle Data Group, K. Nakamura et. al., J. Phys. **G37** (2010) 075021, [http://pdg.lbl.gov/]

[2] T.Feldman, J.Matias, JHEP **0301** (2003) 074, [arXiv:hep-ph/0212158]

[3] ATLAS Collaboration, ATLAS-CONF-2013-038, [http://cds.cern.ch/record/1537961]

[4] CDF Collaboration, Phys.Rev.Lett **106** (2011) 161801, [arXiv:1101.1028]

[5] C. Bobeth, G. Hiller, D. van Dyk, Phys.Rev.D **87** (2012) 034016, [arxiv:1212.2321]

[6] F. Kruger, J. Matias, Phys.Rev.D **71** (2005) 094009, [arXiv:0502060v2]

[7] C. Bobeth, G. Hiller, D. van Dyk, DO-TH 11/02 (2011), [arXiv:1105.2659v1]

[8] LHCb Collaboration, LHCb-CONF-2012-008, [http://cds.cern.ch/record/1427691]

[9] BaBar Collaboration, Phys.Rev.D **71** (2005) 032005, [arXiv:hep-ex/0411016]

[10] BaBar Collaboration, Phys.Rev.D **79** (2009) 031102, [arXiv:0804.4412]

[11] Belle Collaboration, Phys.Rev.Lett. **103** (2009) 171801, [arXiv:0904.0770]

[12] CDF Collaboration, Phys. Rev. Lett. **108** (2012) 081807, [arXiv:1108.0695]